Upper-Hybrid Waves Driven by Meandering Electrons Around Magnetic Reconnection X Line

W.-y. Li, Yu Khotyaintsev, B.-b. Tang, D. Graham, C. Norgren, A. Vaivads, M. André, A. Le, J. Egedal, K. Dokgo, et al.

AGU ADVANCING EARTH AND SPACE SCIENCE

Geophysical Research Letters

RESEARCH LETTER
10.1029/2021GL093164

Key Points:

- Large amplitude nonlinear upper-hybrid (UH) waves are observed on both inflow sides of an X line
- The UH waves are driven by the inbound meandering electrons
- The UH waves may dissipate a significant part of the meandering electron energy gained from the reconnection electric field

Supporting Information:

Supporting Information may be found in the online version of this article.

Correspondence to:

W.-Y. Li and B.-B. Tang,
wyli@spaceweather.ac.cn;
bbtang@spaceweather.ac.cn

Citation:

Li, W.-Y., Khotyaintsev, Y. V., Tang, B.-B., Graham, D. B., Norgren, C., Vaivads, A., et al. (2021). Upper-hybrid waves driven by meandering electrons around magnetic reconnection X line. *Geophysical Research Letters*, *48*, e2021GL093164. https://doi.org/10.1029/2021GL093164

Received 2 MAR 2021
Accepted 8 JUL 2021

Upper-Hybrid Waves Driven by Meandering Electrons Around Magnetic Reconnection X Line

W.-Y. Li[1,2,3], Yu V. Khotyaintsev[3], B.-B. Tang[1], D. B. Graham[3], C. Norgren[4], A. Vaivads[5], M. André[3], A. Le[6], J. Egedal[7], K. Dokgo[8], K. Fujimoto[9], J.-S. He[10], J. L. Burch[8], P.-A. Lindqvist[5], R. E. Ergun[11], R. B. Torbert[12], O. Le Contel[13], D. J. Gershman[14,15], B. L. Giles[14], B. Lavraud[16,17], S. Fuselier[8,18], F. Plaschke[19], C. T. Russell[20], X.-C. Guo[1], Q.-M. Lu[2], and C. Wang[1,21]

[1]State Key Laboratory of Space Weather, National Space Science Center, Chinese Academy of Sciences, Beijing, China, [2]CAS Key Laboratory of Geospace Environment, University of Science and Technology of China, Hefei, China, [3]Swedish Institute of Space Physics, Uppsala, Sweden, [4]Department of Physics and Technology, University of Bergen, Bergen, Norway, [5]Division of Space and Plasma Physics, School of Electrical Engineering and Computer Science, KTH Royal Institute of Technology, Stockholm, Sweden, [6]Plasma Theory and Applications, Los Alamos National Laboratory, Los Alamos, NM, USA, [7]Department of Physics, University of Wisconsin-Madison, Madison, WI, USA, [8]Southwest Research Institute, San Antonio, TX, USA, [9]School of Space and Environment, Beihang University, Beijing, China, [10]School of Earth and Space Sciences, Peking University, Beijing, China, [11]Laboratory of Atmospheric and Space Physics, University of Colorado, Boulder, CO, USA, [12]Space Science Center, University of New Hampshire, Durham, NH, USA, [13]Laboratoire de Physique des Plasmas, CNRS/Ecole Polytechnique/Sorbonne Université/Univ. Paris Sud/Observatoire de Paris, Paris, France, [14]NASA Goddard Space Flight Center, Greenbelt, MD, USA, [15]Department of Astronomy, University of Maryland, College Park, MD, USA, [16]Institut de Recherche en Astrophysique et Planétologie, Université de Toulouse, CNRS, UPS, CNES, Toulouse, France, [17]Laboratoire d'Astrophysique de Bordeaux, Univ. Bordeaux, CNRS, Pessac, France, [18]Department of Physics and Astronomy, University of Texas at San Antonio, San Antonio, TX, USA, [19]Space Research Institute, Austrian Academy of Sciences, Graz, Austria, [20]Department of Earth, Planetary, and Space Sciences, University of California, Los Angeles, CA, USA, [21]School of Astronomy and Space Science, University of Chinese Academy of Sciences, Beijing, China

Abstract Magnetic reconnection is a fundamental process in collisionless space plasma environment, and plasma waves relevant to the kinetic interactions can have a significant impact on the multiscale behavior of reconnection. Here, we present Magnetospheric Multiscale (MMS) observations during an encounter of an X line of symmetric magnetic reconnection in the magnetotail. The X line is characterized by reversals of ion and electron jets and electromagnetic fields, agyrotropic electron velocity distribution functions (VDFs), and an electron-scale current sheet. MMS observe large-amplitude nonlinear upper-hybrid (UH) waves on both sides of the neutral line, and the wave amplitudes have highly localized distribution along the normal direction. The inbound meandering electrons drive the UH waves, releasing the free energy stored from the reconnection electric field along the meandering trajectories. The interaction between the meandering electrons and the UH waves may modify the balance of the reconnection electric field around the X line.

Plain Language Summary The electron-scale kinetic physics in the electron diffusion region (EDR) controls how magnetic field lines break and reconnect. Electron crescent, an indicator of EDR, can drive high-frequency electrostatic waves around EDR. For the first time, the upper-hybrid (UH) waves are observed on both sides of the X line and we show the direct association between the UH waves and the reconnection electric field. The strong wave-electron interaction can change the electron-scale dynamics and may modify the reconnection electric field. This study demonstrates that the UH waves may play an important role in controlling the reconnection rate.

1. Introduction

Magnetic reconnection is a fundamental and universal process whereby the magnetic field energy is transferred to kinetic and thermal energies of charged particles and powers many eruptive processes in space and laboratory plasma environments (Yamada et al., 2010). Magnetic reconnection involves a localized diffusion region, where the magnetic field topology changes by the dissipative electric fields and particle motions

violate the frozen-in condition (Birn et al., 2001; Cai & Lee, 1997; Eastwood et al., 2007; Hesse, Aunai, Birn, et al., 2014; Lavraud et al., 2016; Vasyliunas, 1975). The Magnetospheric Multiscale (MMS) mission was designed and implemented to resolve the electron-scale processes of reconnection in Earth's magnetosphere (Burch, Moore, et al., 2016; Burch, Torbert, et al., 2016; Chen et al., 2019; Fuselier et al., 2017; Torbert et al., 2018; Webster et al., 2018; Zhou et al., 2019).

Waves and turbulence can be generated by magnetic reconnection and produce particle diffusion and anomalous resistivity to feedback on reconnection (Khotyaintsev et al., 2016, 2019; Viberg et al., 2013; Wilder et al., 2019). Recently, plasma-frequency and electro-cyclotron frequency waves in or near the electron diffusion region (EDRs) have been investigated using MMS data. Upper-hybrid (UH) waves (Graham et al., 2017) and electron Bernstein waves (Li et al., 2020) are found to be driven by the agyrotropic crescent-shaped electron VDFs near EDRs of magnetopause reconnection. These waves grow at fast rates and act strongly on electrons to dissipate the unstable electron VDFs. A unified theory shows that the agyrotropic electrons can generate these two types of waves depending on the electron VDFs (Dokgo et al., 2020a). Using a two-dimensional particle-in-cell simulation, Dokgo et al. (2020b) investigate the effects of the UHWs on energy dissipation in the EDR. In the magnetotail, the electron crescents associated with two EDRs (Chen et al., 2019; Torbert et al., 2018) were shown to be responsible for the large-amplitude UH waves (Burch et al., 2019), with nonlinear behavior in the form of electrostatic harmonics. In this letter, we report an X line encounter of symmetric reconnection in the magnetotail, with large-amplitude UH wave observations on both sides of the electron-scale current sheet. Unlike the previous instability analysis based on the electron VDFs, we investigate the direct association between the UH waves and the electron meandering dynamics around the X line. The results suggest that the UH waves may have a significant effect on reconnection electric field.

2. Observations

We investigate MMS observations in the Earth's magnetotail on August 27, 2018. The four MMS spacecraft, located at (−21.1, 11.0, 7.5) Earth radii (R_E) in Geocentric Solar Ecliptic (GSE) coordinates, were in a tetrahedron formation with 34 km average separation. The MMS orbit is shown in the supporting information. We use electric field data from the Electric Double Probes (EDP; Ergun et al., 2016; Lindqvist et al., 2016) and magnetic field data from the FluxGate Magnetometer (FGM; Russell et al., 2016). The particle data are from the Fast Plasma Investigation (FPI; Pollock et al., 2016) and from the mass-resolved instrument Hot Plasma Composition Analyzer (HPCA; Young et al., 2016).

Figures 1a–1d show an overview of the magnetotail observations by MMS1 between 11:40:45 and 11:42:00 UT in GSE coordinates. MMS1 is initially located in the southern lobe region characterized by a large negative B_X and cold plasma with small bulk velocities. At ~11:40:50 UT, MMS1 enters a tailward ion jet with a peak velocity V_{iX} reaching −770 km s^{-1} and sees more energetic (>3 keV) plasma sheet ions. Within the yellow-shaded interval, MMS1 observes an ion jet reversal from tailward to earthward, a small (1.3 nT) magnetic field magnitude near the reversal and a density cavity with a minimum of 0.045 cm^{-3}. After the V_{iX} reversal crossing, MMS1 is located mostly in the earthward ion jet with several neutral line crossings ($B_X \approx 0$ nT).

All four MMS spacecraft observe an intense electron current with an electron jet V_{eX} reversal (near 11:41:26.4 UT) close to the ion jet reversal (Figures 1a–1d). We perform minimum variance analysis (MVA) on **B** and **J** (computed from particle moments) (Paschmann & Daly, 1998) to establish the local coordinate system, which yields **L** = (0.97, −0.17, −0.17; in GSE, close to GSE-**X** direction) along the reconnection magnetic field direction, **M** = (0.20, 0.96, 0.19; close to GSE-**Y** direction) along the X line direction, and **N** = (0.14, −0.22, 0.97; close to GSE-**Z** direction) normal to the current sheet. Figures 1e–1j present a detailed plot of the current sheet from 11:41:21.5 to 11:41:29.5 UT in LMN coordinates. MMS1 observes a B_L reversal (B_L <0 to B_L >0) in the current sheet and an associated E_N reversal. Near these reversals (~11:41:26.4 UT), MMS1 sees a V_{eL} reversal from tailward to earthward directions, a V_{eM} peak and a B_N reversal (B_N <0 to B_N >0), strongly implying that MMS1 encounters an X line. As shown in Figure 1h, MMS1 has extensive observations of agyrotropic electron VDFs over the current sheet crossing, which are interpreted as a strong indicator of EDRs (Burch, Torbert, et al., 2016; Hesse, Aunai, Birn, et al., 2014). Meanwhile, MMS1

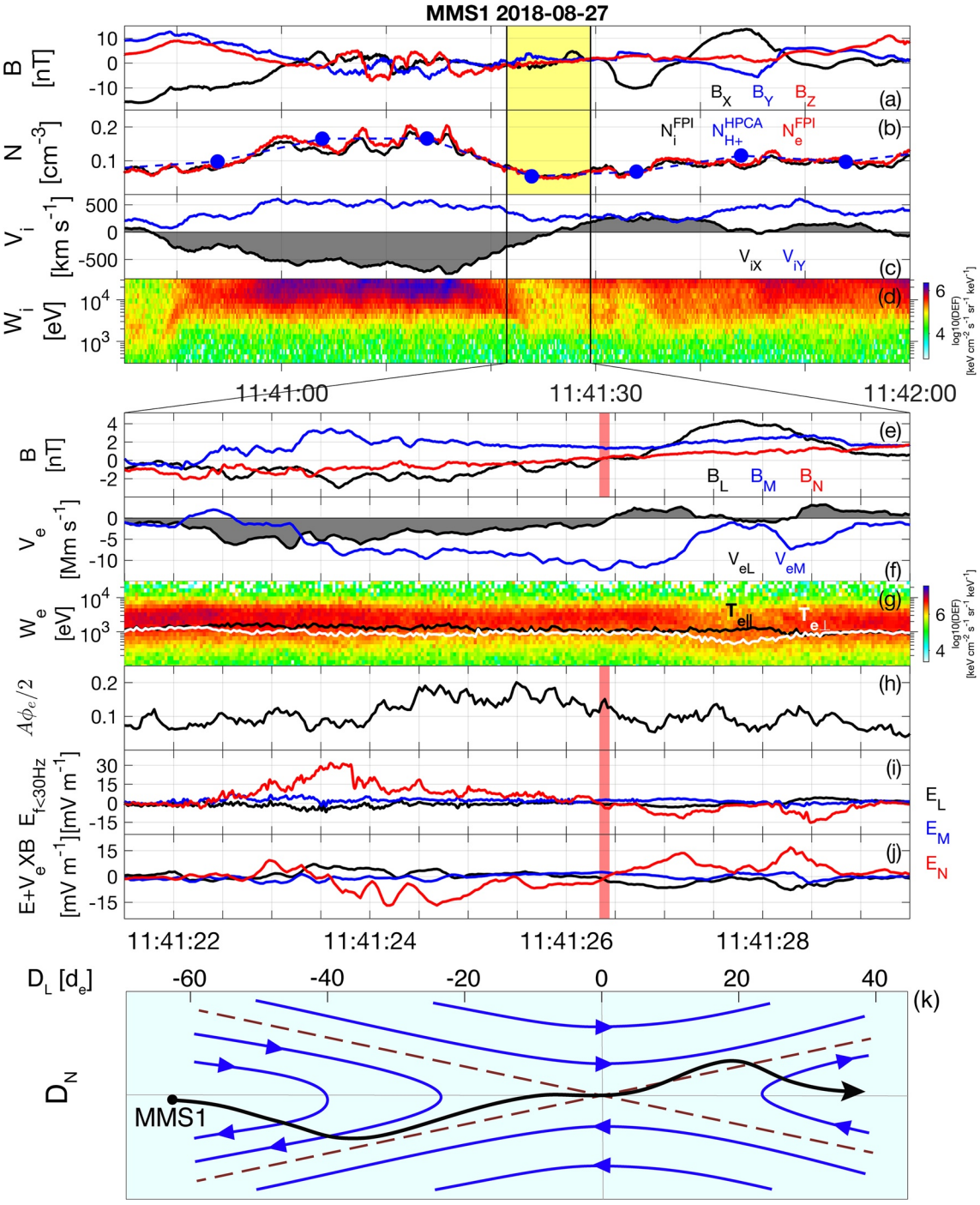

Figure 1. X line encounter by Magnetospheric Multiscale (MMS)1. (a) **B** in Geocentric Solar Ecliptic (GSE). (b) All ion (N_i^{FPI}) and electron (N_e^{FPI}) number densities and hydrogen ion (N_{H+}^{HPCA}) number density. (c) $\mathbf{V}_i$ from Fast Plasma Investigation (FPI). (d) Ion differential energy flux. (e) **B** and (f) $\mathbf{V}_e$ in LMN coordinates. (g) Electron differential energy flux with $T_{e\parallel}$ and $T_{e\perp}$. (h) Agyrotropy measure $A\phi_e$ / 2 (Scudder & Daughton, 2008). (i) **E** with frequencies f < 30 Hz and (j) $\mathbf{E}' = \mathbf{E} + \mathbf{V}_e \times \mathbf{B}$ in LMN. The red vertical bar represents the X line encounter. (k) Schematic of MMS1 trajectory (black curve). The blue arrowed curves denote the magnetic field lines and the dashed lines represent the separatrices.

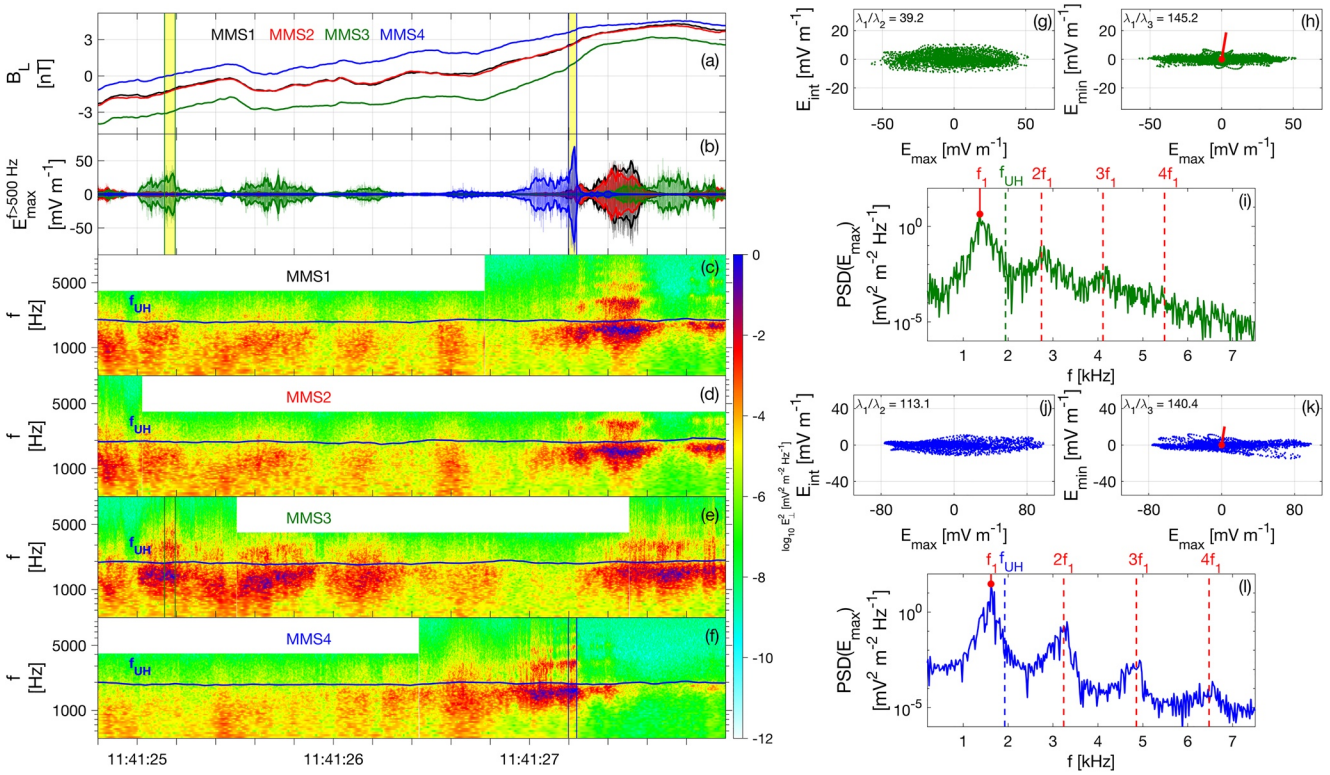

Figure 2. Nonlinear upper-hybrid (UH) waves on both sides of the X line. (a) B_L. (b) High-frequency (f > 500 Hz) E. (c–f) Power spectrogram of $E_\perp$. The yellow bars in (a) and (b) highlight two examples of the UH waves from Magnetospheric Multiscale (MMS)3 and MMS4. Wave analysis on the MMS3 example: Hodograms of (g) E_{max} versus E_{int} and (h) E_{max} versus E_{min} and (i) wave power spectrum of E_{max}. E_{max}, E_{int}, and E_{min} are the electric fields in the maximum, intermediate, and minimum variance directions from minimum variance analysis (MVA). In (i), the frequency f_l of the peak corresponding to the maximum power is $0.71f_{UH}$. Wave analysis on the MMS4 example is presented in (j–l). In (l), f_l equals $0.84f_{UH}$.

observes significant electric field in the electron rest frame ($E' = \mathbf{E} + \mathbf{V}_e \times \mathbf{B}$, Figure 1j), which is consistent with kinetic particle-in-cell simulations (i.e., Hesse, Aunai, Birn, et al., 2014; Shay et al., 2016; Zenitani et al., 2017). All these features indicate that MMS1 encounters an X line in the magnetotail.

Timing analysis (Paschmann & Daly, 1998) of the B_N reversal indicates that the X line moves tailward with a velocity $V_L^{X-line} \sim -350$ km s^{-1}. At the X line, the out-of-plane electron flow peaks at $V_{eM} = -12{,}300$ km s^{-1} at the location of the V_{eL} reversal. Toward the tail side of the X line, the electron outflow speed $|V_{eL}|$ increases and $|V_{eM}|$ decreases gradually. V_{eL} reaches a peak of $-7{,}200$ km s^{-1} at 11:41:23.2 UT when $|V_{eM}|$ approaches zero. Then, the vanishing of E' illustrates that electrons in the exhaust couple back to the reconnected magnetic field lines (Figure 1j). Toward the Earth side of the X line (right side of the plot), MMS1 observes a decrease of the electron flow. Near 11:41:27.7 UT, the spacecraft moves to the inflow region, mainly seen in a relatively large B_L (4.3 nT), a small $\mathbf{V}_e$, and a large electron temperature anisotropy $T_{e\parallel}/T_{e\perp} = 2.8$ (Figure 1g), which is a characteristic signature of the inflow region in the EDR vicinity (Chen et al., 2008; Egedal et al., 2012, 2013). Figure 1k shows a sketch of an inferred MMS1 trajectory through the EDR, where $d_e = 25$ km is the electron inertial length. The Debye length λ_D is approximately 1.0 km. The observed current sheet can be modeled by a Harris current sheet (Harris, 1962), and its half-width is 1.4 d_e (see the supporting information for details). The guide field B_G is 1.4 nT near the X line.

Figures 2b–2f show the waveform and the wave power spectrogram of the high-frequency **E** fluctuations. As shown in Figures 2c–2f, wave power peaks below the local UH frequencies, but shows several higher frequency harmonics above f_{UH}. Here, $f_{UH} = \sqrt{f_{pe}^2 + f_{ce}^2} \sim f_{pe}$, where f_{pe} is the electron plasma frequency, f_{ce} is the electron cyclotron frequency, and $f_{pe} \gg f_{ce}$ due to weak magnetic fields. As shown by two examples in Figure 2, the high-frequency **E** have well-defined maximum variance directions based on MVA of the waveform. The waveform is one-dimensional (1D), linearly polarized, and nearly perpendicular to **B**. Above

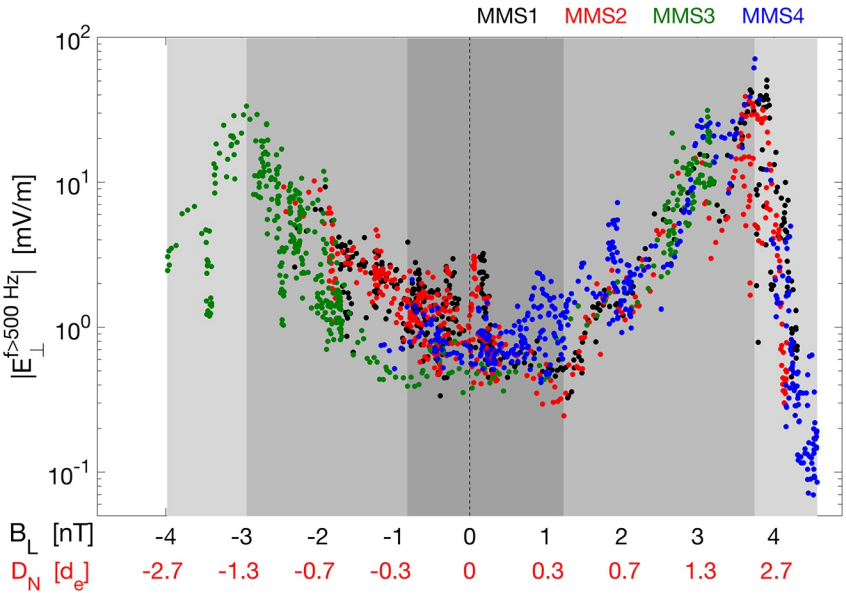

Figure 3. Localized upper-hybrid (UH) waves along B_L and D_N. The scatter plot of the nonlinear UH wave amplitudes is presented here at the cadence of 7.8 ms (FluxGate Magnetometer [FGM] resolution), and the shadows generally denote different regions of the localized UH waves.

f_{UH}, there are several harmonics with power peaks near the harmonics of f_i. All the features suggest that the waves are nonlinear UH waves with harmonics, likely produced by nonlinear beam-plasma interactions (Burch et al., 2019; Dokgo et al., 2019; Yoon et al., 2003).

Figure 2 shows that the nonlinear UH waves are observed on both sides of the neutral line near the X line. Here, we investigate the spatial distribution of the wave amplitudes along the normal direction of the current sheet. Figure 3 displays the scatter plot of the wave envelope amplitudes versus B_L and the distance along **N** (D_N). The UH wave amplitudes form an M-shaped distribution along D_N: the peak amplitudes are located near $-1.2d_e$ on the southern side and $+2.0d_e$ on the northern side, and the amplitudes decrease quickly toward the neutral line, with low amplitudes (0.5–1 mV m^{-1}) around the neutral line.

Previous works have extensively studied the generation mechanism of the large-amplitude UH waves in and near the EDRs and find that the agyrotropic crescent-shaped electron VDFs generate the observed UH waves (Burch et al., 2019; Dokgo et al., 2019, 2020a; Graham et al., 2017). The electrostatic property of the UH waves indicates that the wave unit vectors $\hat{\mathbf{k}}$ are in the E_{max} directions and the signs of $\hat{\mathbf{k}}$ are determined by the electron crescent. As shown in Figure 4c, $\hat{\mathbf{k}}$ on the southern side are generally along **−L**, **−M**, and **+N** directions and $\hat{\mathbf{k}}$ on the northern side are along **+L**, **−M**, and **−N** directions. This indicates that the UH waves propagate toward the neutral line.

Figures 4f–4s display selected reduced two-dimensional (2D) electron VDFs from the northern to the southern sides. To show the association between the electron VDFs and the UH wave propagation directions, we choose the V_B-V_k and V_k-$V_{\perp 2}$ planes to display the reduced 2D VDFs. As shown in Figures 4i and 4p, MMS1 sees enhanced electron VDFs along the **−B** direction near the X line, where **B** is dominated by B_M. This antiparallel electron flow is consistent with acceleration by a reconnection electric field $E_R \approx E_M > 0$ (Norgren et al., 2016). On either side of the neutral line, MMS observe a combination of counter-streaming inflow electrons along **B** (Chen et al., 2008; Egedal et al., 2012, 2013) and electron crescents. The angular widths and phase space densities of the crescents decrease gradually with D_N. The angular spread of the electron crescents are roughly symmetric across $V_N = 0$ (red lines in Figures 4m-4o and 4q-4s). The angular width and the phase space density of the electron crescent at $D_N = 2.7d_e$ (Figures 4f and 4m) are relatively small, implying the northern boundary of all the meandering trajectories.

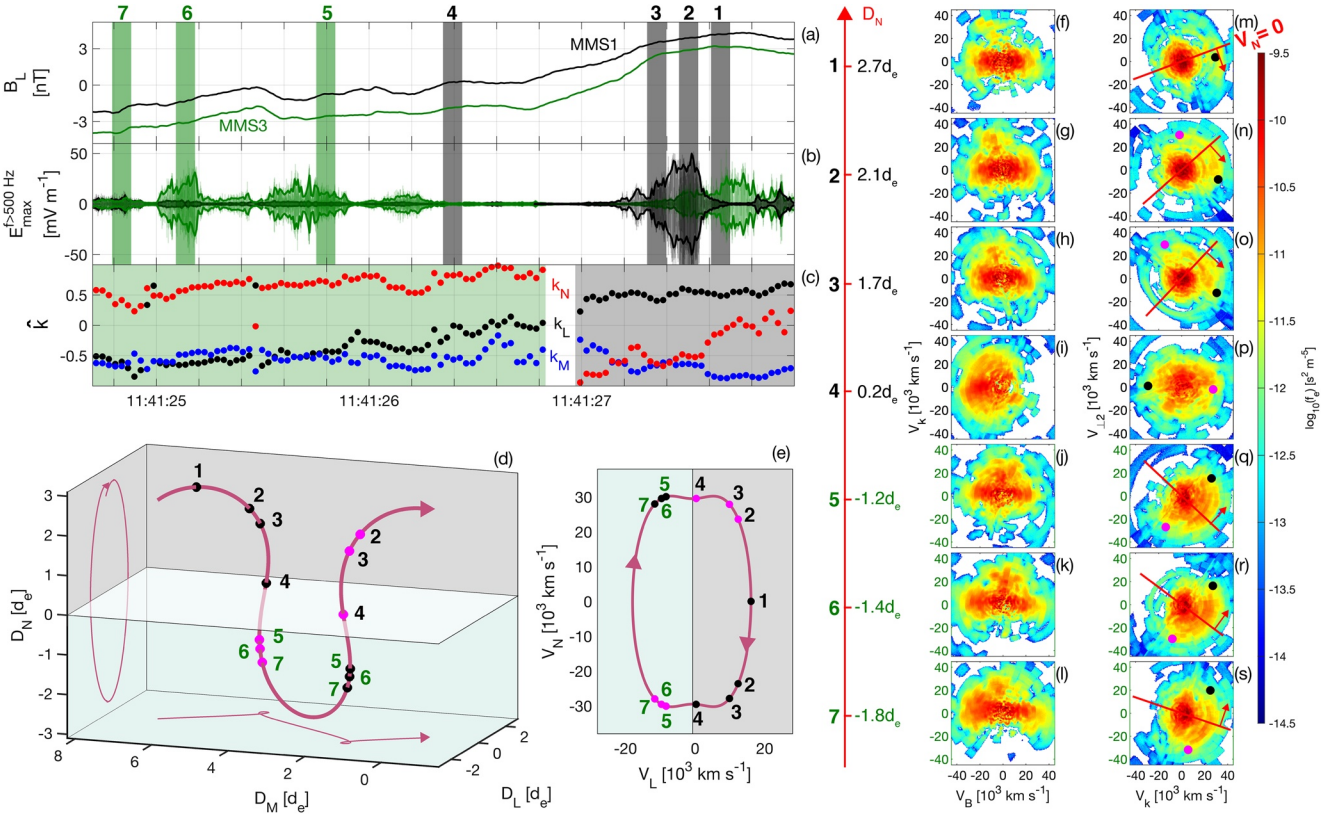

Figure 4. Upper-hybrid (UH) waves driven by the inbound meandering electrons. (a) B_L. (b) High-frequency (f > 500 Hz) E. (c) $\hat{\mathbf{k}}$. The green and black shadows highlight $\hat{\mathbf{k}}$ on the southern (by Magnetospheric Multiscale [MMS]3) and northern (by MMS1) sides. An example of electron meandering trajectories in (d) real space and (e) V_L-V_N velocity space. (f–s) Two-dimensional reduced electron velocity distribution functions (VDFs) at the times indicated by the vertical bars (from right to left) in (a) and (b). The red arrowed lines point toward the neutral line. The black and magenta dots are explained in the text.

Around the X line, the crescent at one location is formed by the superposition of electrons in different phases of their meandering motions (i.e., Shay et al., 2016). Since we observe only wave unit vectors pointing toward the neutral line, it suggests that the wave growth might be associated with crescent electrons in a certain meandering phase. Therefore, we investigate the direct relation between the UH waves and the meandering electrons. We start by considering the meandering motion of an electron with its turning point at $D_N = 2.7d_e$. The starting point of this example trajectory is shown as the black dot in Figure 4m, which represents the crescent part with a positive gradient along V_k. Figures 4d and 4e display its meandering trajectory in real space and velocity space using the model Harris current sheet (see the Supporting Information) with B_G and the observed E_N. The L-direction motion of the meandering trajectory comes from B_G and yields k_L. The meandering trajectory contributes to different parts of the electron VDFs at different locations. The black and magenta dots in Figures 4n–4s correspond to the inbound and outbound parts of this meandering trajectory at different D_N. The UH waves are associated with the $+V_N$ meandering electrons on the southern side (Figures 4q–4s) and with the $-V_N$ meandering electrons on the northern side (Figures 4m–4o). This denotes that the UH waves on both sides of the neutral line are driven by the inbound meandering electrons around the X line.

For the electron crescents, the largest positive gradients along V_k are at $1.5–2.5 \times 10^4$ km s^{-1}, which provides a good estimation of the phase speed of the UH waves (Burch et al., 2019; Graham et al., 2017). The fundamental frequencies are approximately 1.5 kHz. Thus, the UH wavelength is estimated to be 10–17 km (0.4–0.7 d_e, 9.8–16.7 λ_D), which is consistent with the previous linear theory results (Dokgo et al., 2019; Graham et al., 2017). The maximum wave electric Φ is estimated to be 170 V. In the wave frame, the UH waves can trap a significant portion of electrons with perpendicular speeds between $\pm\sqrt{2q_e\Phi / m_e} = \pm 7.7 \times 10^3$ km s^{-1}, and the free energy in the electron VDFs is dissipated via Landau damping process.

3. Discussion

E_N accelerates the neutral line electrons toward the inflow region, meanwhile they are accelerated along the meandering trajectories by E_R (Bessho et al., 2018; Horiuchi & Sato, 1994; Torbert et al., 2018). At one location, the inbound meandering electrons get more acceleration than the outbound electrons by E_R, which makes the crescent VDFs asymmetric across $V_N = 0$ (Bessho et al., 2018). Here, we estimate the acceleration energy by E_R and the UH wave energy to evaluate whether the acceleration energy of the inbound electrons by E_R can be responsible for the observed UH waves. The energy density gain of the inbound meandering electrons by E_R is estimated to be

$$U_{RE} \approx e\langle E_R\rangle D_M^{me} N_e \alpha \approx (4.5-20)\times 10^{-15} Jm^{-3}. \quad (1)$$

here, $\langle E_R\rangle \approx 1-1.5$ mV m^{-1} is the average E_R during the meandering motions, $D_M^{me} \approx 1-3d_e$ is the characteristic meandering distance along **M**, and N_e is the electron number density. $\alpha \approx 2.5\%$ is the density ratio of the inbound electrons, which is estimated by following a similar method in Norgren et al. (2016). The average energy density of the UH waves is estimated to be

$$U_{UHW} = \frac{1}{D_{N2}-D_{N1}} \int_{D_{N1}}^{D_{N2}} \frac{1}{2}\epsilon_0 \delta \mathbf{E}^2 dD_N \approx 5.6\times 10^{-15} Jm^{-3}, \quad (2)$$

where $D_{N1} = 0.4d_e$ and $D_{N2} = 2.7d_e$ are the integral boundaries for the northern side. The estimated energy density gain of the inbound meandering electrons are comparable, but larger than the estimated wave energy density, $U_{RE} \geq U_{UHW}$. This means that the UH waves may dissipate a significant part of the energy gain of the meandering electrons from E_R. The dissipated energy may scatter and thermalize the inbound meandering electrons. The crescent VDF observed at one location needs to be interpreted as the integrated results of the UH wave-electron interaction from the meandering turning locations to the observation location. This effect can change the gradient of the electron pressure tensor off-diagonal terms. Thus, the whole process may potentially modify the balance of the reconnection electric field (Cai & Lee, 1997; Egedal et al., 2019; Hesse, Aunai, Birn, et al., 2014; Hesse, Aunai, Sibeck, & Birn, 2014; Vasyliunas, 1975). So far, the two X-line encounters (20170711 and the current ones) with large-amplitude UH waves are both observed in the magnetotail and have weak guide fields. For reconnection under variant plasma and magnetic field conditions in different regions, the existence and effect of the UH waves still need more efforts from both observational and numerical simulation aspects.

4. Summary

We report an X-line encounter of symmetric magnetic reconnection with a guide field B_G/B_L of 0.09 in Earth's magnetotail. We find large-amplitude nonlinear UH waves on both sides of the electron-scale current sheet. The UH waves are driven by the inbound meandering electrons around the X line, and their amplitudes form an M-shaped distribution in the direction normal to the current sheet. The UH waves may dissipate a significant part of the energy gain of the meandering electrons from E_R. The interaction between the meandering electrons and the UH waves may modify the reconnection electric field.

Acknowledgments
This work was supported by NNSFC Grant No. 41731070, 41974170, 41974196, and 41874189, the Chinese Academy of Sciences (QYZDJSSW-JSC028, XDA15052500, XDA17010301, and XDB41000000), and the Specialized Research Fund for State Key Laboratories of China. W.-Y. Li was also supported by the Youth Innovation Promotion Association (2018177), the Young Elite Scientists Sponsorship Program by CAST, and the Open Research Program of Key Laboratory of Geospace Environment CAS. CN received support from the Research Council of Norway under contract 30086. The authors appreciate the fruitful discussion with Kaijun Liu and Jian Yang from Southern University of Science and Technology, Shenzhen, China.

Data Availability Statement

The authors thank the MMS team and instrument principal investigators for data access and support. All data used in this work are available at the MMS Data Center (https://lasp.colorado.edu/mms/sdc/public/).

References

Bessho, N., Chen, L.-J., Wang, S., & Hesse, M. (2018). Effect of the reconnection electric field on electron distribution functions in the diffusion region of magnetotail reconnection. *Geophysical Research Letters*, *45*(22), 12142–12152. https://doi.org/10.1029/2018gl081216

Birn, J., Drake, J. F., Shay, M. A., Rogers, B. N., Denton, R. E., Hesse, M., et al. (2001). Geospace environmental modeling (GEM) magnetic reconnection challenge. *Journal of Geophysical Research*, *106*(A3), 3715–3719. https://doi.org/10.1029/1999ja900449

Burch, J. L., Dokgo, K., Hwang, K., Torbert, R., Graham, D., Webster, J., et al. (2019). High-frequency wave generation in magnetotail reconnection: Linear dispersion analysis. *Geophysical Research Letters*, *46*, 4089–4097. https://doi.org/10.1029/2019gl082471

Burch, J. L., Moore, T. E., Torbert, R. B., & Giles, B. L. (2016). Magnetospheric Multiscale overview and science objectives. *Space Science Reviews*, *199*(1), 5–21. https://doi.org/10.1007/s11214-015-0164-9

Burch, J. L., Torbert, R. B., Phan, T. D., Chen, L.-J., Moore, T. E., Ergun, R. E., et al. (2016). Electron-scale measurements of magnetic reconnection in space. *Science*, *352*(6290), aaf2939. https://doi.org/10.1126/science.aaf2939

Cai, H. J., & Lee, L. C. (1997). The generalized Ohm's law in collisionless magnetic reconnection. *Physics of Plasmas*, *4*(3), 509–520. https://doi.org/10.1063/1.872178

Chen, L.-J., Bessho, N., Lefebvre, B., Vaith, H., Fazakerley, A., Bhattacharjee, A., et al. (2008). Evidence of an extended electron current sheet and its neighboring magnetic island during magnetotail reconnection. *Journal of Geophysical Research*, *113*(A12). https://doi.org/10.1029/2008ja013385

Chen, L.-J., Wang, S., Hesse, M., Ergun, R. E., Moore, T., Giles, B., et al. (2019). Electron diffusion regions in magnetotail reconnection under varying guide fields. *Geophysical Research Letters*, *46*(12), 6230–6238. https://doi.org/10.1029/2019gl082393

Dokgo, K., Hwang, K.-J., Burch, J. L., Choi, E., Yoon, P. H., Sibeck, D. G., & Graham, D. B. (2019). High-frequency wave generation in magnetotail reconnection: Nonlinear harmonics of upper hybrid waves. *Geophysical Research Letters*, *46*, 7873–7882. https://doi.org/10.1029/2019gl083361

Dokgo, K., Hwang, K.-J., Burch, J. L., Yoon, P. H., Graham, D. B., & Li, W. (2020a). High-frequency waves driven by agyrotropic electrons near the electron diffusion region. *Geophysical Research Letters*, *47*(5), e2020GL087111. https://doi.org/10.1029/2020gl087111

Dokgo, K., Hwang, K.-J., Burch, J. L., Yoon, P. H., Graham, D. B., & Li, W. (2020b). The Effects of Upper-Hybrid Waves on Energy Dissipation in the Electron Diffusion Region. *Geophysical Research Letters*, *47*(19), e2020GL089778. https://doi.org/10.1029/2020GL089778

Eastwood, J. P., Phan, T.-D., Mozer, F. S., Shay, M. A., Fujimoto, M., Retinò, A., et al. (2007). Multi-point observations of the hall electromagnetic field and secondary island formation during magnetic reconnection. *Journal of Geophysical Research*, *112*(A6). https://doi.org/10.1029/2006ja012158

Egedal, J., Daughton, W., & Le, A. (2012). Large-scale electron acceleration by parallel electric fields during magnetic reconnection. *Nature Physics*, *8*(4), 321–324. https://doi.org/10.1038/nphys2249

Egedal, J., Le, A., & Daughton, W. (2013). A review of pressure anisotropy caused by electron trapping in collisionless plasma, and its implications for magnetic reconnection. *Physics of Plasmas*, *20*(6), 061201. https://doi.org/10.1063/1.4811092

Egedal, J., Ng, J., Le, A., Daughton, W., Wetherton, B., Dorelli, J., et al. (2019). Pressure tensor elements breaking the frozen-in law during reconnection in earth's magnetotail. *Physical Review Letters*, *123*, 225101. https://doi.org/10.1103/PhysRevLett.123.225101

Ergun, R. E., Tucker, S., Westfall, J., Goodrich, K. A., Malaspina, D. M., Summers, D., et al. (2016). The axial double probe and fields signal processing for the MMS mission. *Space Science Reviews*, *199*(1–4), 167–188. https://doi.org/10.1007/s11214-014-0115-x

Fuselier, S. A., Vines, S. K., Burch, J. L., Petrinec, S. M., Trattner, K. J., Cassak, P. A., et al. (2017). Large-scale characteristics of reconnection diffusion regions and associated magnetopause crossings observed by mms. *Journal of Geophysical Research: Space Physics*, *122*(5), 5466–5486. https://doi.org/10.1002/2017JA024024

Graham, D. B., Khotyaintsev, Y. V., Vaivads, A., Norgren, C., André, M., Webster, J. M., et al. (2017). Instability of agyrotropic electron beams near the electron diffusion region. *Physical Review Letters*, *119*, 025101. https://doi.org/10.1103/PhysRevLett.119.025101

Harris, E. G. (1962). On a plasma sheath separating regions of oppositely directed magnetic field. *Il Nuovo Cimento - B* (1955-1965), *23*(1), 115–121. https://doi.org/10.1007/BF02733547

Hesse, M., Aunai, N., Birn, J., Cassak, P., Denton, R. E., Drake, J. F., et al. (2014). Theory and modeling for the magnetospheric multiscale mission. *Space Science Reviews*, *199*(1), 1–54. https://doi.org/10.1007/s11214-014-0078-y

Hesse, M., Aunai, N., Sibeck, D., & Birn, J. (2014). On the electron diffusion region in planar, asymmetric, systems. *Geophysical Research Letters*, *41*(24), 8673–8680. https://doi.org/10.1002/2014GL061586

Horiuchi, R., & Sato, T. (1994). Particle simulation study of driven magnetic reconnection in a collisionless plasma. *Physics of Plasmas*, *1*(11), 3587–3597. https://doi.org/10.1063/1.870894

Khotyaintsev, Y. V., Graham, D. B., Norgren, C., Eriksson, E., Li, W., Johlander, A., et al. (2016). Electron jet of asymmetric reconnection. *Geophysical Research Letters*, *43*(11), 5571–5580. https://doi.org/10.1002/2016GL069064

Khotyaintsev, Y. V., Graham, D. B., Norgren, C., & Vaivads, A. (2019). Collisionless magnetic reconnection and waves: Progress review. *Frontiers in Astronomy and Space Sciences*, *6*(70). https://doi.org/10.3389/fspas.2019.00070

Lavraud, B., Zhang, Y. C., Vernisse, Y., Gershman, D. J., Dorelli, J., Cassak, P. A., et al. (2016). Currents and associated electron scattering and bouncing near the diffusion region at earth's magnetopause. *Geophysical Research Letters*, *43*(7), 3042–3050. https://doi.org/10.1002/2016GL068359

Li, W. Y., Graham, D. B., Khotyaintsev, Y. V., Vaivads, A., André, M., Min, K., et al. (2020). Electron Bernstein waves driven by electron crescents near the electron diffusion region. *Nature Communications*, *11*(1), 141. https://doi.org/10.1038/s41467-019-13920-w

Lindqvist, P.-A., Olsson, G., Torbert, R. B., King, B., Granoff, M., Rau, D., et al. (2016). The spin-plane double probe electric field instrument for MMS. *Space Science Reviews*, *199*(1–4), 137–165. https://doi.org/10.1007/s11214-014-0116-9

Norgren, C., Graham, D. B., Khotyaintsev, Y. V., André, M., Vaivads, A., Chen, L.-J., et al. (2016). Finite gyroradius effects in the electron outflow of asymmetric magnetic reconnection. *Geophysical Research Letters*, *43*(13), 6724–6733. https://doi.org/10.1002/2016GL069205

Paschmann, G., & Daly, P. W. (1998). *Analysis methods for multi-spacecraft data*. ESA Publications Division.

Pollock, C., Moore, T., Jacques, A., Burch, J., Gliese, U., Saito, Y., et al. (2016). Fast plasma investigation for Magnetospheric Multiscale. *Space Science Reviews*, *199*(1–4), 331–406. https://doi.org/10.1007/s11214-016-0245-4

Russell, C. T., Anderson, B. J., Baumjohann, W., Bromund, K. R., Dearborn, D., Fischer, D., et al. (2016). The Magnetospheric Multiscale Magnetometers. *Space Science Reviews*, *199*(1–4), 189–256. https://doi.org/10.1007/s11214-014-0057-3

Scudder, J., & Daughton, W. (2008). "Illuminating" electron diffusion regions of collisionless magnetic reconnection using electron agyrotropy. *Journal of Geophysical Research*, *113*(A6), A06222. https://doi.org/10.1029/2008JA013035

Shay, M. A., Phan, T. D., Haggerty, C. C., Fujimoto, M., Drake, J. F., Malakit, K., et al. (2016). Kinetic signatures of the region surrounding the X line in asymmetric (magnetopause) reconnection. *Geophysical Research Letters*, *43*(9), 4145–4154. https://doi.org/10.1002/2016GL069034

Torbert, R. B., Burch, J. L., Phan, T. D., Hesse, M., Argall, M. R., Shuster, J., et al. (2018). Electron-scale dynamics of the diffusion region during symmetric magnetic reconnection in space. *Science*, *362*(6421), 1391–1395. https://doi.org/10.1126/science.aat2998

Vasyliunas, V. M. (1975). Theoretical models of magnetic field line merging. *Reviews of Geophysics*, *13*(1), 303–336. https://doi.org/10.1029/RG013i001p00303

Viberg, H., Khotyaintsev, Y., Vaivads, A., André, M., & Pickett, J. (2013). Mapping hf waves in the reconnection diffusion region. *Geophysical Research Letters*, *40*(6), 1032–1037. https://doi.org/10.1002/grl.50227

Webster, J. M., Burch, J. L., Reiff, P. H., Daou, A. G., Genestreti, K. J., Graham, D. B., et al. (2018). Magnetospheric multiscale dayside reconnection electron diffusion region events. *Journal of Geophysical Research: Space Physics*, *123*(6), 4858–4878. https://doi.org/10.1029/2018ja025245

Wilder, F. D., Ergun, R. E., Hoilijoki, S., Webster, J., Argall, M. R., Ahmadi, N., et al. (2019). A survey of plasma waves appearing near dayside magnetopause electron diffusion region events. *Journal of Geophysical Research: Space Physics*, *124*(10), 7837–7849. https://doi.org/10.1029/2019ja027060

Yamada, M., Kulsrud, R., & Ji, H. (2010). Magnetic reconnection. *Reviews of Modern Physics*, *82*(1), 603–664. https://doi.org/10.1103/RevModPhys.82.603

Yoon, P. H., Gaelzer, R., Umeda, T., Omura, Y., & Matsumoto, H. (2003). Harmonic Langmuir waves. I. Nonlinear dispersion relation. *Physics of Plasmas*, *10*(2), 364–372. https://doi.org/10.1063/1.1537238

Young, D. T., Burch, J. L., Gomez, R. G., De Los Santos, A., Miller, G. P., Wilson, P., et al. (2016). Hot plasma composition analyzer for the magnetospheric multiscale mission. *Space Science Reviews*, *199*(1), 407–470. https://doi.org/10.1007/s11214-014-0119-6

Zenitani, S., Hasegawa, H., & Nagai, T. (2017). Electron dynamics surrounding the X line in asymmetric magnetic reconnection. *Journal of Geophysical Research: Space Physics*, *122*(7), 7396–7413. https://doi.org/10.1002/2017JA023969

Zhou, M., Deng, X. H., Zhong, Z. H., Pang, Y., Tang, R. X., El-Alaoui, M., et al. (2019). Observations of an electron diffusion region in symmetric reconnection with weak guide field. *The Astrophysical Journal*, *870*(1), 34. https://doi.org/10.3847/1538-4357/aaf16f